Version of Record: https://www.sciencedirect.com/science/article/pii/S0925838822030055
Manuscript_0153034d5e7165e87b3c21b53ad46b08

New insights in GeTe growth mechanisms

Guillaume Roland[a,b], Alain Portavoce[a], Maxime Bertoglio[a], Marion Descoins[a], Jacopo Remondina[a], Didier Dutartre[b], Frédéric Lorut[b], Magali Putero[*,a]

* Corresponding author.

Email address: magali.putero@univ-amu.fr (Magali Putero)

© 2022 published by Elsevier. This manuscript is made available under the Elsevier user license
https://www.elsevier.com/open-access/userlicense/1.0/

[a] AixMarseille Univ, CNRS, Campus Scientifique de St Jérôme, IM2NP UMR7334, 13397, Marseille cedex 20, France

[b] STMicroelectronics, 850 rue Jean Monnet, 38920, Crolles, France

Abstract

The compound GeTe, despite its simple stoichiometry, is rather unconventional and has been investigated both from a fundamental and technological perspective: it is of high interest for several technologies such as data-storage (phase change memories) and thermoelectricity. The understanding of GeTe growth is thus a key issue for technological applications and fundamental understanding. In this work, GeTe crystallization kinetics is compared to Ge/Te reactive diffusion kinetics using in situ X-ray diffraction measurements, as well as in situ transmission electron microscopy. GeTe crystallization from an amorphous solid solution exhibiting the stoichiometry of the compound GeTe is found to occur at the same temperature as for the reactive diffusion of an amorphous Ge layer on top of a polycrystalline Te layer. Furthermore, GeTe growth is of tridimensional type in the two cases, and can be modeled by the Johnson-Mehl-Avrami-Kolmogorov model. Using this model, the activation energies of nucleation and growth were determined for both crystallization and reactive diffusion. The results suggest that GeTe exhibits nucleation/reaction kinetics unusually low compared to atomic transport kinetics, contrasting with other germanides.

Keywords: GeTe, Phase Change Materials, crystallization, reactive diffusion, in situ X-Ray diffraction, in situ TEM, thin film

1. Introduction

Phase Change Random Access Memory (PCRAM) is one of the most promising technology for the next generation of non-volatile memories with Ferroelectric RAM and Magnetic RAM [1]. PCRAM exploits the surprising phase change properties of Phase Change Materials (PCM) in order to achieve a memory effect. PCM can reversibly and quickly change between a high-resistivity amorphous (and in general low-reflectivity) state and a low-

resistivity crystalline (and in general high-reflectivity) state through thermal annealing [2–5]. This class of materials is mostly composed of chalcogenides glasses [2,5] , and has been used for nonvolatile optical memories such as CDs, DVDs and Blu-ray discs, using the large reflectivity difference between the two states [2,3,5,6]. Ge-Sb-Te based chalcogenide alloys or compounds (GST) are considered to be among the most promising PCM for PCRAM applications [2,5,6]. However, their low crystallization temperatures (~ 150-170°C for $Ge_2Sb_2Te_5$ [5]) can be a limiting factor for industrial production and high reliability applications, such as automotive applications [7,8]. In contrast, the binary compound GeTe exhibits ultra-fast switching as well as a higher crystallization temperature than GST (~ 180-230°C depending on oxidation [9]). Consequently, GeTe is also a strong PCM contender for PCRAM applications [4], but is also considered as a good candidate for the development of GeTe-based RF switches [10–12]. Furthermore, numerous studies have also reported interesting GeTe properties for thermoelectric applications [13–15].

Both nucleation and growth mechanisms can have a significant impact on applications. In PCRAM for example, amorphous region crystallization is the slowest process and hence determines the maximum speed of the SET operation. GeTe growth mechanism is known to be growth-dominated, allowing high switching speed once nucleation has occurred [4]. However, depending on interfaces, nucleation and growth can be different, leading to different device properties. Thus, the control of the GeTe compound growth is of prime importance for all applications. Two main techniques are commonly used in industrial processes for the solid-state production of thin film compounds: i) reactive diffusion between two films in contact [16–18] , which is driven by atomic transport and interfacial reaction, or ii) non-diffusive reaction [19] that is also called “crystallization”, since it consists in the formation of an ordered compound from a homogeneous solid solution in the amorphous state exhibiting the stoichiometry of the desired compound. GeTe crystallization has been mainly studied to date from homogeneous Ge(50%):Te(50%) amorphous (a-GeTe) thin films for PCRAM applications [20,21]. The crystallization of a-GeTe thin films is characterized by homogeneous random nucleation of the GeTe compound, followed by its three-dimensional (3D) growth [9,20,22]. Reported GeTe crystallization experiments were performed using differential scanning calorimetry (DSC) [23,24], in situ resistivity measurements [25–27] or in situ reflectivity measurements [22,23,28], allowing an activation energy linked to the crystallization process to be determined using the Kissinger analysis. This activation energy varies between 1.7 and 3.9 eV depending on the authors and the experimental technique [22–

25,28]. Reactive diffusion (RD) is commonly used to produce silicide and germanide ohmic contacts on the source, the drain and the gate of microelectronic transistors in the complementary-metal-oxide-semiconductor (CMOS) technology through the self-aligned-silicide (Salicide) process, based on the RD of a metallic film with the semiconductor [16–18]. RD depends on interfacial reaction and self-diffusion [29–31]. Thus, RD experiments can allow the kinetics of semiconductor/metal reaction and atomic transport to be assessed, which are of main interest for crystallization understanding and process simulation [29]. Germanide RD on flat substrates generally leads to a two-dimensional (2D) growth [31–35], characterized by first an interfacial nucleation step leading to the extremely fast formation of an interfacial thin layer of few nanometers-thick (lateral growth), followed by the growth of this 2D layer in the direction perpendicular to the interface (normal growth). The growth of the layer can be simulated by linear-parabolic type of models [30], reproducing the compound linear growth versus time, limited by interfacial reaction kinetics, for small layer thicknesses, followed by a parabolic growth regime versus time, limited by atomic transport kinetics, once the growing layer has reached a critical thickness [29,31]. However, only parabolic growth has been so far observed in the case of 2D germanide growth [31], meaning that germanium/metal reaction kinetics is generally several orders of magnitude faster than grain boundary self-diffusion kinetics in the compound.

In this work, GeTe crystallization kinetics in a 150 nm-thick a-GeTe thin film is compared to the GeTe growth kinetics observed during the RD of a 60 nm-thick Ge layer deposited on a 90 nm-thick Te layer using in situ X-ray diffraction (XRD) and in situ transmission electron microscopy (TEM). Surprisingly, GeTe follows a 3D growth exhibiting similar nucleation temperatures in the two cases. Activation energies of nucleation and growth are determined using the Johnson-Mehl-Avrami-Kolmogorov (JMAK) model [36–38] to fit in situ XRD measurements acquired during isotherms.

2. Material and methods

The samples were elaborated in a commercial magnetron sputtering system exhibiting a base pressure of 10^{-8} mbar. Te was sputtered from a 99.99% pure Te-target in RF mode, while Ge was sputtered from a 99.999% pure Ge-target in DC mode, using a 99.9999% pure

Ar gas flow under a work pressure of 3.6×10^{-3} mbar. Ge and Te fluxes were calibrated separately by measuring the thickness of sputtered films deposited at room temperature (RT) on the native oxide of Si(001) substrates by X-ray reflectivity. Two types of samples were elaborated. Sample #1 was meant to study GeTe crystallization. In this case, Ge and Te were co-deposited in the Ge(50 at.%):Te(50 at.%) stoichiometry at RT on the native SiO_2 layer (~ 2 nm-thick) of a Si(001) substrate. The SiO_2 layer is kept as a diffusion barrier preventing Si atoms from the substrate to interact with the deposited layers. The 150 nm-thick GeTe layer was capped with 10 nm of pure Ge at the same temperature. The Ge layer was added aiming to limit the GeTe layer oxidation. The entire film was fully amorphous after deposition (Fig. 1). Sample #2 was destined for the study of solid state Ge/Te RD. To this aim, a 90 nm-thick Te layer was deposited on the same substrate as used for sample #1, before to be covered by a 70 nm-thick Ge layer. All the layers were deposited at RT, and the sputtering powers and deposition times were kept the same as for sample #1. The reaction of the entire bilayer is expected leading to the formation of a GeTe layer of same thickness as after the entire crystallization of sample #1, with an extra 10 nm-thick layer of a-Ge on the surface.

After deposition, the samples (6×6 cm^2) were cut into several pieces. 1.5×1.5 cm^2 specimens were used to performed in situ XRD measurements. The specimens were annealed at constant temperature (isothermal annealing) or following a heating ramp (isochronal annealing) *in situ* in a XRD setup under a vacuum of ~ 10^{-5} mbar. All the XRD measurements were performed in the Bragg-Brentano geometry (θ–2θ) on a Panalytical Empyrean diffractometer equipped with an PIXcel detector designed for high speed data collection, using a Cu K-α source (λ = 0.154 nm). For isochronal annealing, the heating ramp was performed between 100°C and 350°C following a temperature ramp of 10°C per minute steps separated by 4.5 minute-long XRD scans at constant temperature, corresponding to an average heating ramp of ~ 0.9 K min^{-1}. Scans were executed every 5°C. Four to five isotherms between 145°C and 190°C were performed on each type of samples, in addition to the ramp annealing.

In situ TEM observations gave complementary information on the growth of the GeTe phase during Ge/Te RD. A TEM lamella has been prepared using the in-situ lift out technique in a FIB-SEM system, Helios450™ from ThermoFisher, and mounted onto a molybdenum grid. Final thinning of the lamella has been done using a 8kV acceleration voltage, in order to limit the possible FIB Gallium induced amorphization. Once prepared, the grid has been mounted onto a sample heating holder from Gatan, and then loaded into a Tecnai F20 TEM,

from ThermoFisher, operating at a 200kV accelerating voltage in TEM bright field mode. The in situ TEM annealing starts at RT up to 350°C following several isothermal steps. During each isothermal step, one image was taken every minute. The total annealing time was about 1 hour and 40 minutes.

3. Results and discussion

3.1. GeTe growth during isochronal annealing

Fig. 1(a) presents series of XRD patterns recorded during the ramp annealing of sample #1 (GeTe layer) as a function of temperature. No diffraction peak is detected in this sample before annealing. The sample is entirely amorphous. Upon heating, two peaks simultaneously appear at $2\theta = 29.75°$ and 42.28° when reaching $T = 170°C$. They respectively correspond to the (202) and (024) Bragg reflections of the rhombohedral α-GeTe phase. Ge crystallization is detected at $T = 290°C$ with the apparition of the Ge(111) diffraction peak at $2\theta = 27.31°$ and coincides with an intensity increase of the diffraction peak α-GeTe(202).

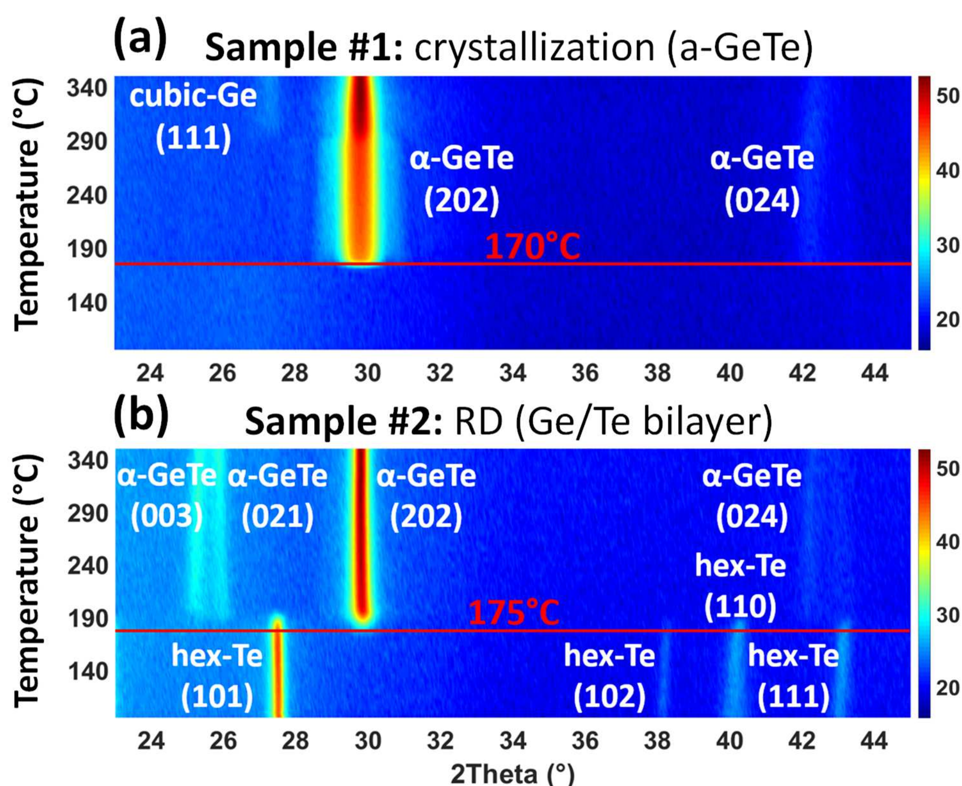

Fig. 1: XRD patterns (λ = 0.154 nm) as a function of temperature acquired during in situ isochronal annealing of ~ 0.9 K min^{-1} for a) sample #1 (GeTe layer) and b) sample #2 (Ge/Te bilayer). The color plot panel is in counts/s.

Fig. 2 presents the variations of the normalized integrated XRD intensities versus annealing temperature. The signal is proportional to the corresponding phase diffracting volume [39]. Only the peak α-GeTe(202) (open circles) is presented in the case of sample #1: the Ge(111) peak intensity is very low, and thus, shows significant fluctuations preventing getting reliable data after integration. Fig. 2 shows also the average grain size L of α-GeTe along the normal of the sample surface, determined from the full width at half maximum (FWHM) w of the α-GeTe(202) peak according to the Scherrer formula, and neglecting the microstrain contribution:

$$L = \frac{k \times \lambda}{w \times cos(\theta)} \tag{1}$$

with the factor k = 0.89 in our case. GeTe grain size reaches rapidly a maximum L ~ 12 nm during GeTe growth (T < 200 °C) and stays almost constant, following the diffraction intensity up to 290°C. At this temperature, both α-GeTe volume (XRD integrated intensity) and grain size (L) are found to increase again. Our results are in agreement with similar studies previously reported: the GeTe crystallization temperature (i.e. nucleation temperature) T_n = 170 °C is in agreement with the literature for uncapped layers [40], and the subsequent intensity increase of the peak α-GeTe(202) concurrently with Ge crystallization was already observed and discussed [27], meaning that the GeTe layer is probably slightly Ge-rich.

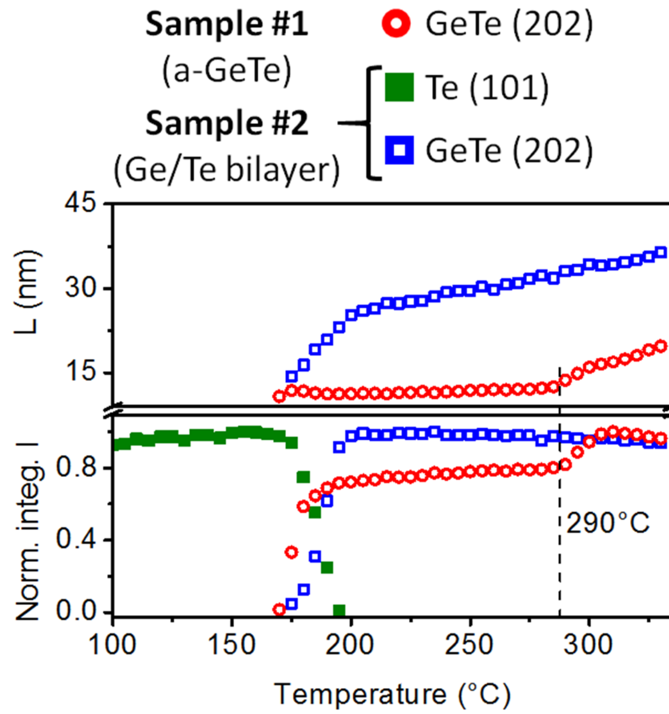

Fig. 2: Normalized integrated intensities of diffraction peaks and average grain size (*L*) during in situ XRD isochronal annealing of ~ 0.9 K min^{-1}: sample #1 (GeTe layer), α-GeTe(202) (open circles); and sample #2 (Ge/Te bilayer), hexagonal-Te(101) (solid squares) and α-GeTe(202) (open squares).

Fig. 1(b) presents the series of XRD patterns acquired during the ramp annealing of sample #2 (Ge/Te bilayer). Four diffraction peaks are already observed before annealing at $2\theta = 27.53°$, 38.16°, 40.16° and 43.07°, respectively corresponding to the Bragg reflections (101), (102), (110) and (111) of the hexagonal Te phase. The as-deposited Te layer is polycrystalline (poly-Te). No diffraction peaks are observed from the Ge layer, as this layer is amorphous (a-Ge) after deposition. Upon annealing, the vanishing of Te peaks coincides with the simultaneous appearance at T = 175°C of the four diffraction peaks α-GeTe(003), α-GeTe(021), α-GeTe(202), and α-GeTe(024), respectively at 2θ = 25.21°, 25.98°, 29.83°, and 42.16°. Despite the structural and chemical distribution differences between sample #1 and sample #2, the α-GeTe phase is found to form at the same temperature (in the 5°C measurement error) in the two samples. However, despite that the peak α-GeTe(202) is the most intense in the two samples, the samples exhibit different textures, as the peaks α-GeTe(003) and α-GeTe(021) are detected only in sample #2, exhibiting higher diffraction intensities than the peak α-GeTe(024) in this case. Those differences may be linked to the different nucleation type in the two samples: nucleation should be homogeneous within the

amorphous GeTe layer in sample #1, while it occurs at the Ge/Te interface in sample #2. The Te layer being polycrystalline in this case (a-Ge/poly-Te bilayer), this layer may influence the texture of the growing GeTe grains. Furthermore, Ge crystallization is not observed during Ge/Te RD in sample #2 despite the presence of the 70 nm-thick a-Ge layer, contrasting with GeTe crystallization in sample #1. This could be due either to a better stoichiometric total composition for sample #2 and/or to the fact that for this sample, the Ge excess is not within the GeTe crystalline layer at the end of the reaction, meaning that Ge may not find the necessary nucleus sites (i.e. GeTe grain boundaries) to initiate heterogeneous crystallization at low temperature.

Fig. 2 shows typical phase volume variations during 2D growth of compounds by RD [41]: the diffraction intensity of the reacting layers (here only Te since Ge stays amorphous) decreases concurrently with the increase of the growing compound diffraction intensity (i.e. α-GeTe). The superimposition in Fig. 2 of the variations of the diffraction peak α-GeTe(202) in the two samples during the same annealing shows that despite a similar nucleation temperature T_n = 170°C, GeTe growth kinetics are different during crystallization and RD. Indeed, growth kinetics are expected to be different as GeTe growth does not need atomic transport in sample #1 (the composition is homogeneous and corresponds to the GeTe stoichiometry), while GeTe growth during RD depends on atomic transport kinetics [30,31]. Average GeTe grain size is larger in sample #2, and its evolution with temperature differs from sample #1: L increases with the GeTe phase volume up to ~ 200 °C during RD; at that temperature, the GeTe volume has reached a maximum, but L is still increasing with temperature following a slower rate, reaching L ~ 36 nm at the end of the experiment. This behavior is in agreement with a growth regime below 200°C, followed by grain growth competition at higher temperature. The grain size difference observed between the two samples (bigger grains for sample #2, Fig.2) is probably related to a difference of nucleation site density in the two samples: GeTe nucleation should be homogeneous within the entire layer in sample #1, promoting a large number of nuclei, and thus, leading to smaller grain sizes (grain growth competition). Instead, nucleation starts at the Ge/Te interface in sample #2, promoting a significantly smaller number of nuclei and bigger isolated grains, such as the columnar grain observed in Fig. 5c and 5d.

3.2. GeTe growth during isothermal annealing

Fig. 3 presents the variations of the α-GeTe(202) XRD normalized integrated intensity recorded during different isothermal annealing of sample #1 (Fig. 3(a)) and sample #2 (Fig. 3(b)) between T = 145 and 190 °C. The signal is proportional to the crystallized α-GeTe phase volume, so to the crystallized fraction. For sample #1, the α-GeTe crystallization fraction can be fitted with the JMAK model, as expected. However, the GeTe growth in sample #2 cannot be simulated using typical linear-parabolic 2D growth models [30,42]. Instead, GeTe growth in sample #2 can also be fitted with the JMAK model. In this model, the crystallized fraction (or the phase volume) variation with time $f(t)$ follows the law:

$$f(t) = 1 - \exp(-\kappa \times t^n) \quad (2)$$

κ includes the product of the nucleation rate with the growth rate, and n is generally called the Avrami coefficient. According to this model, κ is constant if the nucleation rate $N = N_0 \exp(-E_n/k_B T)$ and the growth rate $\nu = \nu_0 \exp(-E_g/k_B T)$ are constant versus time at constant temperature (k_B is the Boltzmann constant). This is the case for GeTe growth in the two samples #1 and #2 (Fig. 3). In particular, Fig. 3(c) and Fig. 3(d) show that GeTe growth occurs according to a same regime at low temperature, between 145 and 160°C (n ~ 4) for sample #1 and between 145 and 175°C (n ~ 2.5) for sample #2, while the growth regime changes (i.e. the value of n changes) and eventually cannot be fitted by the JMAK model at high temperatures. The value of n can have different interpretations, including a dependence on the geometry of the growing phase (2D or 3D for example) or a dependence on the nucleation site density and its saturation [43,44].

GeTe growth during crystallization is known to follow a 3D growth [9,20] , which is in agreement with n = 4 in the JMAK model, considering the homogeneous growth of spherical nucleus in a nucleation-and-growth regime. In this case:

$$\kappa(T) = \kappa_0 \exp(-\frac{E_a}{k_B T}) \quad (3)$$

And $E_a = E_n + (n-1) E_g$ (4)

is the activation energy of nucleation and growth.

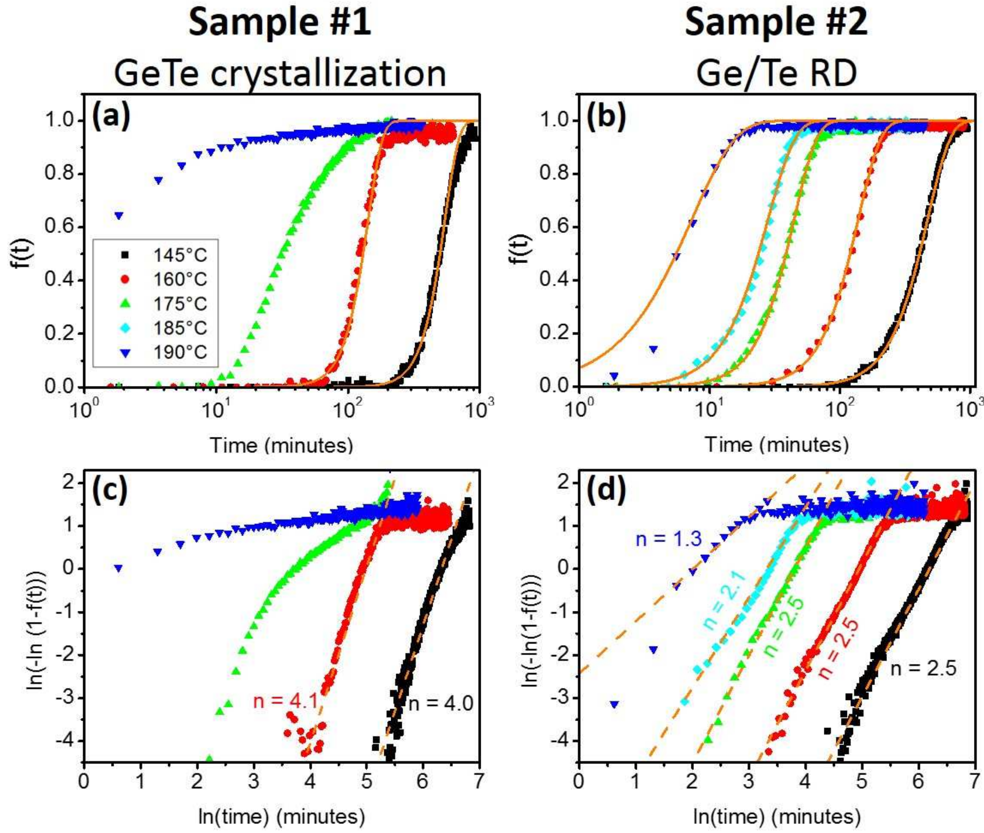

Fig. 3: Normalized integrated intensity $f(t)$ of the α-GeTe(202) diffraction peak versus time recorded during in situ XRD isothermal annealing at various temperatures between 145°C and 190°C: a) and c) sample #1 (GeTe layer); b) and d) sample #2 (Ge/Te bilayer). The solid line in a) and b) corresponds to a fit using the JMAK model with the Avrami exponent n determined from the corresponding signal $\phi = \ln(-\ln(1 - f(t)))$ in c) and d).

Fig. 4(a) presents the plot of κ versus $1/k_BT$ using the logarithmic scale determined from the in situ XRD signals measured from sample #1 (Fig. 3(a)) at the two temperatures 145°C and 160°C (n ~ 4), and from sample #2 at three temperatures. Considering sample #1, the activation energy of nucleation and growth was found to be E_a = 6.23 eV. The nucleation time Δt corresponding to the time needed to detect for the first time the diffraction signal during isothermal annealing informs on the nucleation kinetics, and was described as follows:

$$\frac{1}{\Delta t} = \Omega \times \exp(-\frac{E_n}{k_BT}) \qquad (5)$$

Table 1 presents the different nucleation time measured for each sample.

Table 1: Nucleation time Δt measured during isothermal annealing for samples #1 and #2.

Isothermal temperature (°C)	Nucleation time Δt (s)	
	Sample #1 Crystallization	**Sample #2 Reactive Diffusion**
145	13325	5935
160	2475	1817
175	549	581

Fig. 4(b) presents the variations of Δt measured from the in situ XRD signals acquired from sample #1 at T = 145°C, 160°C, and 175 °C (extracted from Fig. 3(a)) versus $1/k_B T$. The activation energy of nucleation for GeTe crystallization was found to be E_n = 1.72 eV, giving an activation energy of growth from eq. (4) $E_g = 1/3(E_a - E_n)$ = 1.50 eV. The activation energies determined from Kissinger analyses (isochronal annealing) during GeTe crystallization were found to be comprised between 1.7 and 3.9 eV [22–25,28]. This large energy range could be linked to both the small composition variations reported in the different studies and the effect of uncontrolled incorporation of impurities such as carbon and oxygen, depending on sputtering conditions (target purity, argon gas pressure and purity, deposition speed…) [45]. It is interesting to note that the activation energy of nucleation reported in the present work is comprised in the range, 1.7 and 3.9 eV, reported in the bibliography. This observation is in agreement with Navarro et al. [25] suggesting that the activation energy determined from Kissinger analyses should correspond to the activation energy of the nucleation process due to the very fast GeTe growth.

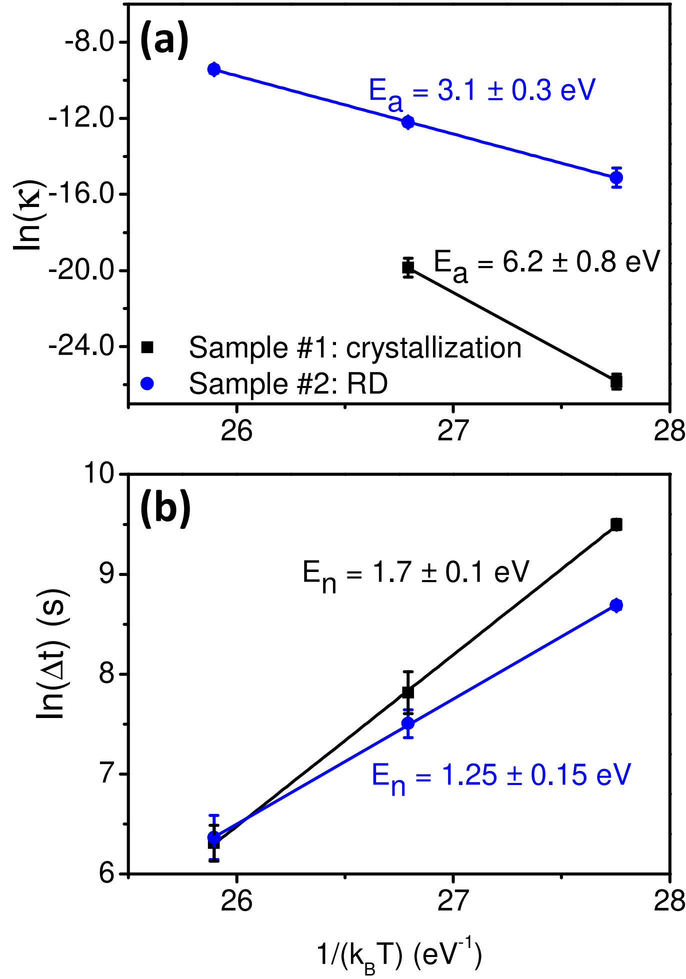

Fig. 4: Variations of a) the parameter ln(κ) and b) the nucleation time ln(Δt) according to the inverse of temperature for sample #1 (GeTe layer) and sample #2 (Ge/Te bilayer).

The interpretation of the GeTe growth following eq.(2) in sample #2 is less straightforward since n ~ 2.5 in this case. Thus, *in situ* TEM observations were performed aiming to determine the GeTe growth mode in sample #2.

Figure 5 presents four subsequent TEM images acquired during the in situ heating of a cross-section TEM lamella prepared from sample #2 from RT to T = 225°C. The blue dotted arrows are used to mark identical locations in the different images, and the red solid arrow shows the evolution of a growing GeTe grain within amorphous Ge. After deposition (Fig. 5(a)), the sample is made of the stack of a 63 nm-thick amorphous Ge layer on top of a 80 nm-thick polycrystalline Te layer. One can note that no intermixing layer is observed at the a-Ge/poly-Te interface. Generally, a 3-to-5 nm-thick intermixing layer is formed between the metal and Si or Ge during RT sputtering [31,33]. This layer can be amorphous or crystalline and acts as the initial stage of 2D growth of silicides or germanides [31]. During heating (Fig. 5(b) to 5(d)), polycrystalline GeTe starts to grow between Ge and Te. The FFT (Fig. 5e)

performed on the large grain observed in Fig. 5d allowed two different distances to be measured, 3.56 nm and 3.42 nm, corresponding respectively to the (003) and (021) planes of the rhombohedral GeTe phase. However, GeTe does not form a continuous layer between the a-Ge and poly-Te layers as usually observed for germanide growth [31–35,41]. Instead, in sample #2 the GeTe grain 3D growth occurs both in the a-Ge layer and in the poly-Te layer in comparable proportions. Fig. 6 shows a schematic illustration of the growth process: GeTe nucleation starts at the Ge/Te interface (Fig.6a) without the need for atomic transport. GeTe formation leads to the presence of a-Ge/GeTe and GeTe/Te interfaces (Fig.6b). If the GeTe nuclei would have formed a continuous 2D layer between a-Ge and poly-Te thanks to a fast lateral growth, GeTe growth would have been piloted by Ge and Te diffusion in GeTe grain boundaries (GB), as for usual germanide and silicide thin film reactive diffusion. However, the GeTe nuclei being isolated and the temperature being relatively low for bulk diffusion (see ref. [46] and [47] for Ge and Te self-diffusion), atomic transport can occur at this stage both in GeTe GB (arrows 1 in Fig. 6b) and at interfaces (arrows 2 in Fig. 6b). The contribution of interface diffusion is obvious in the poly-Te layer, as TEM images show GeTe growth along Te grain boundaries (Fig.5), and can explain why isolated GeTe grains can grow in a-Ge (Fig. 5c). Thus, after nucleation, GeTe 3D growth results from concurrent growths in a-Ge and poly-Te via Te diffusion at the a-Ge/GeTe interface in a-Ge and Ge diffusion in GB and at the GeTe/Te interface in Te (Fig. 6b), as well as from Ge and Te GB self-diffusion in poly-GeTe. The growth occurring almost simultaneously in a-Ge and poly-Te according to in situ TEM observations (Fig. 5), diffusion kinetics seems to be comparable at these different interfaces. The reason for the slower growth kinetics of GeTe nuclei along the a-Ge/Te interface needs to be investigated, as one could expect similar diffusivity at the a-Ge/Te interface. Despite that the GeTe growth is 3D, after a given time (shorter at higher temperature), GeTe will eventually form a continuous rough polycrystalline region separating remaining a-Ge and poly-Te as depicted in Fig.6c. From this stage, GeTe growth can go on using only Ge and Te GB diffusion through the GeTe layer, up to the entire Ge/Te reaction, leading in our case to a full polycrystalline GeTe layer as shown in Fig. 6d. This scenario suggests a possible change of growth kinetics from a first stage mediated by atomic diffusion in both GeTe GB and inter-phases, to a second stage mediated by GeTe GB diffusion only, which could explain the variations of the Avrami exponent with temperature observed in Fig. 3d.

These observations are in agreement with the GeTe growth kinetic observed by in situ XRD in this sample: GeTe growth does not follow the usual 2D growth modeled by linear-parabolic growth models, but corresponds to a 3D growth that can be modeled by the JMAK model. The fact that n is different from 4 could be linked to different effects. For example, the nucleation rate and nucleus distribution are probably different in the amorphous Ge layer and in the polycrystalline Te layer. Furthermore, n should take into account that the growth rate in sample #2 is dependent of atomic transport kinetics following a $t^{1/2}$ law. According to TEM observations, GeTe growth in sample #2 can be modeled using the JMAK model with the same assumptions as for sample #1, with also $E_a = E_n + (n-1)E_g$ in this case. Similar to the case of sample #1, the variations of κ determined from the in situ XRD signals measured from sample #2 (Fig. 3(b)) at T = 145°C, 160°C, and 175°C (n ~ 2.5) are presented in Fig. 4(a) versus $1/k_BT$. The activation energy of nucleation and growth was found to be E_a = 3.1 eV.

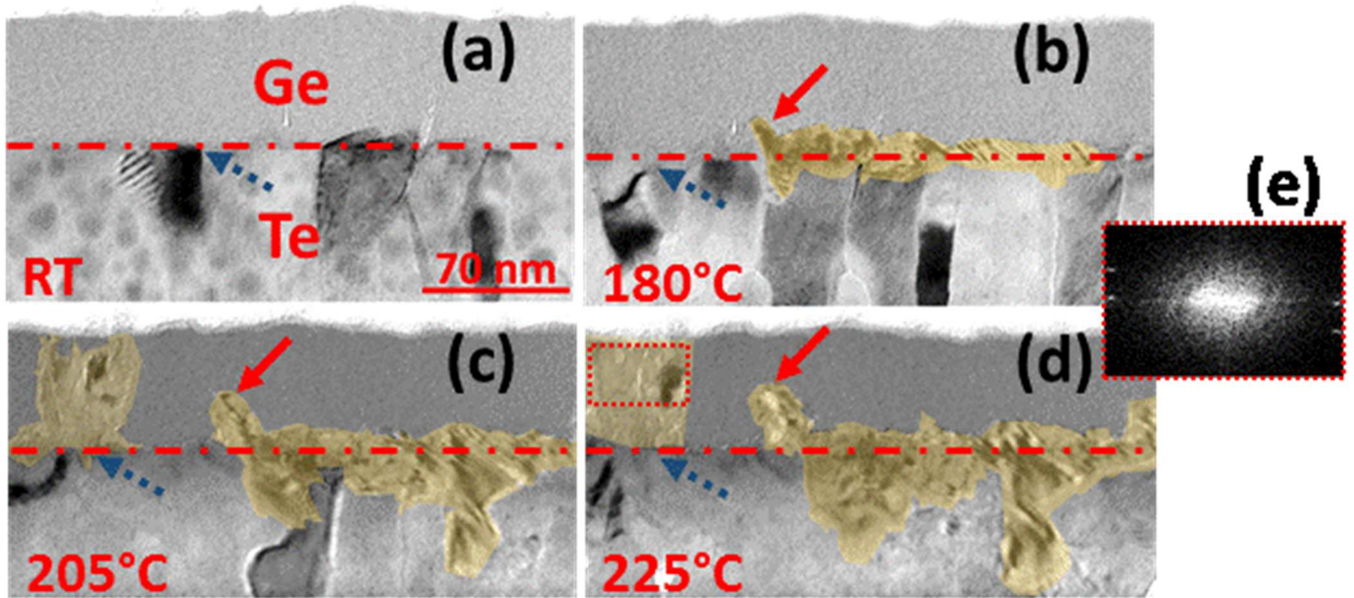

Fig. 5: Cross-section TEM images acquired during in situ sample #2 (Ge/Te) heating from RT to 225°C: a) RT, b) 180°C, c) 205°C, d) 225°C and (e) FFT and reciprocal distances measured in the red dotted rectangle. The blue dotted arrow is used to mark identical location in the different images, and the red solid arrow shows the evolution of a growing GeTe grain within the amorphous Ge layer. The added color highlights the new phase.

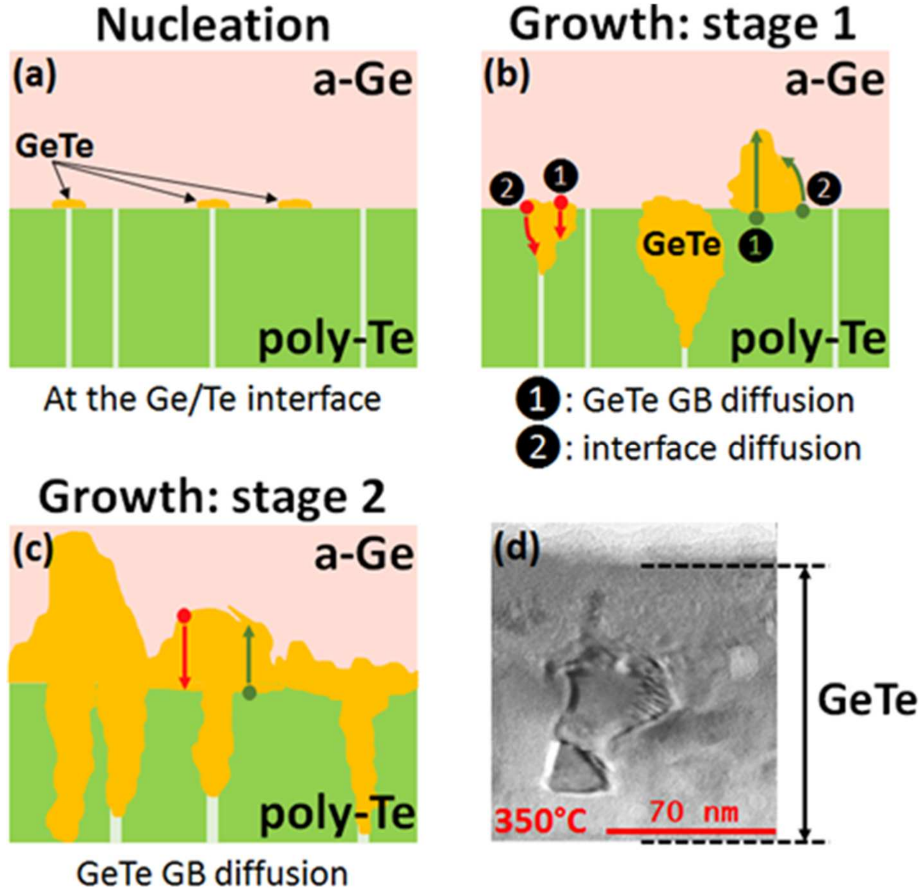

Fig. 6: (a), (b) and (c): schematic illustration of nucleation and growth in sample #2 (Ge/Te bilayer, RD); (d) Cross-section TEM images acquired during in situ sample #2 (Ge/Te) heating at 350°C: almost all the layer is crystalline.

Table 2: Activation energies determined from in situ XRD isotherms using the JMAK model.

Sample	E_a (eV)	E_n (eV)	E_g (eV)
#1-crystallization	6.2 ± 0.8	1.7 ± 0.1	1.50 ± 0.3
#2-RD	3.1 ± 0.3	1.25 ± 0.15	1.21 ± 0.4

The variations of Δt measured from the same in situ XRD signals are presented in Fig. 4(b). The activation energy of nucleation for GeTe RD was found to be E_n = 1.25 eV, giving an activation energy of growth E_g = 1.21 eV. Tab. 2 summarizes the activation energies determined from the isothermal in situ XRD measurements performed at low temperature (≤ 175 °C), using the JMAK model. These activation energies of nucleation and growth are

difficult to compare with the data available in the literature. Indeed, quantitative data concerning interfacial reaction for the system Ge-Te are lacking, as well as data concerning self-diffusion, especially in grain boundaries and in amorphous solid solutions. Comparing with silicides growth via RD, which has been more studied than germanides, one can note that GeTe nucleation energy is higher than the usual activation energy of reaction (0.8 eV for Ni_2Si [29], 0.9 eV for Ni_5Ge_3 [41] for example), and GeTe growth energy is of same order as for silicides effective self-diffusion during RD (1.5 eV for Ni_2Si [29] for example). The activation energy of nucleation is found ~40% higher in the homogeneous GeTe amorphous solid solution than at the a-Ge/poly-Te interface. Furthermore, the nucleation time is shorter for RD below 175°C (see Fig. 4(b)). This behavior is probably related to the different nature of nucleation in the two cases: homogeneous in amorphous GeTe and heterogeneous at the a-Ge/poly-Te interface. The activation energy of growth is found about 24% higher for GeTe crystallization from the stoichiometric amorphous solid solution compared to RD from the a-Ge/poly-Te bilayer. However, growth kinetics is faster for crystallization (see Fig. 2 and Fig. 3), as expected. Indeed, crystallization growth kinetics should correspond to the "atom ordering" process, while RD should consist of both atomic transport (atom diffusion in grain boundaries and interfaces) and "atomic ordering" (i.e. reaction). One can note that the difference of growth kinetics between crystallization and RD is not that significant (Fig. 2) and $E_n \geq E_g$ during GeTe RD, suggesting that nucleation (or reaction) may be the limiting process for GeTe RD, instead of self-diffusion for most of other germanides. The fact that the activation energy of growth is found lower during RD could be linked to point defect injection during RD. Indeed, atomic transport is in general several orders of magnitude faster during RD compared to equilibrium diffusion [48]. This effect has been suggested to be due to point defect injection during low-temperature RD [48–51].

4. Conclusion

GeTe crystallization has been compared to Ge/Te reactive diffusion aiming to improve our knowledge of GeTe growth mechanisms using in situ XRD measurements and in situ TEM observations. GeTe crystallization temperature was found to be T_n = 170 °C ± 5 °C during isochronal annealing of ~ 0.9 K min^{-1} in agreement with the literature. GeTe was found to follow a two-steps-crystallization including Ge crystallization as already reported in former investigations. The Ge crystallization observed during GeTe crystallization is probably

linked to a mechanism involving the second step of GeTe crystallization as they occur simultaneously, but also because Ge crystallization is not observed during Ge/Te RD despite the presence of the tenth-of-nanometer-thick a-Ge layer. GeTe formation during isochronal RD occurs at the same temperature as GeTe crystallization (T_n = 175 °C ± 5°C). However, GeTe growth kinetics as well as the GeTe texture are different between crystallization and RD, and GeTe grain size is about the double for RD at the end of annealing. Isothermal annealing shows that GeTe crystallization and RD correspond to a 3D growth that can be modeled by the JMAK model. This model allowed the activation energies of nucleation and growth to be determined for the two processes. Comparisons between kinetics and activation energies of crystallization and RD show that GeTe is different from usual germanides: it follows a 3D growth instead of a 2D growth during RD, which can be due to a peculiarly fast atomic transport kinetics compared to reaction (i.e. nucleation) kinetics.

Sample CRediT author statement

Guillaume Roland: Investigation, Validation, Formal analysis, Data Curation, Visualization, Writing-Original Draft. **Alain Portavoce**: Conceptualization, Methodology, Writing – Original Draft and review& editing, Supervision, Project Administration, Funding acquisition. **Maxime Bertoglio:** Investigation, Methodology. **Marion Descoins**: Methodology, Writing – review& editing. **Jacopo Remondina:** Investigation, Validation, Formal analysis. **Didier Dutartre**: Project administration, Validation. **Frédéric Lorut:** Investigation, Methodology, Project administration. **Magali Putero**: Conceptualization, Methodology, Writing – review& editing, Supervision, Project Administration, Funding acquisition.

Acknowledgements

This project was supported by the French National Association of Research and Technology (ANRT Project 2020/0907).

Reference

[1] M.H.R. Lankhorst, B.W.S.M.M. Ketelaars, R.A.M. Wolters, Low-cost and nanoscale non-volatile memory concept for future silicon chips, Nat. Mater. 4 (2005) 347–352. doi:10.1038/nmat1350.

[2] S. Raoux, G.W. Burr, M.J. Breitwisch, C.T. Rettner, Y.C. Chen, R.M. Shelby, M. Salinga, D. Krebs, S.H. Chen, H.L. Lung, C.H. Lam, Phase-change random access memory: A scalable technology, IBM J. Res. Dev. 52 (2008) 465–479. doi:10.1147/rd.524.0465.

[3] M. Wuttig, N. Yamada, Phase-change materials for rewriteable data storage., Nat. Mater. 6 (2007) 824–32. doi:10.1038/nmat2009.

[4] G. Bruns, P. Merkelbach, C. Schlockermann, M. Salinga, M. Wuttig, T.D. Happ, J.B. Philipp, M. Kund, Nanosecond switching in GeTe phase change memory cells, Appl. Phys. Lett. 95 (2009) 043108. doi:10.1063/1.3191670.

[5] P. Noé, C. Vallée, F. Hippert, F. Fillot, J.-Y. Raty, Phase-change materials for non-volatile memory devices: from technological challenges to materials science issues, Semicond. Sci. Technol. 33 (2018) 13002. doi:10.1088/1361-6641/aa7c25.

[6] N. Yamada, Origin, secret, and application of the ideal phase-change material GeSbTe, Phys. Status Solidi Basic Res. 249 (2012) 1837–1842. doi:10.1002/pssb.201200618.

[7] S. Privitera, E. Rimini, R. Zonca, Amorphous-to-crystal transition of nitrogen- and oxygen-doped Ge 2Sb2Te5 films studied by in situ resistance measurements, Appl. Phys. Lett. 85 (2004) 3044–3046. doi:10.1063/1.1805200.

[8] E. Gomiero, G. Samanni, J. Jasse, C. Jahan, O. Weber, R. Berthelon, R. Ranica, L. Favennec, V. Caubet, D. Ristoiu, J.P. Reynard, L. Clement, P. Zuliani, R. Annunziata, F. Arnaud, Crystallization Speed in Ge-Rich PCM Cells as a Function of Process and Programming Conditions, IEEE J. Electron Devices Soc. 7 (2019) 517–521. doi:10.1109/JEDS.2019.2913467.

[9] R. Berthier, N. Bernier, D. Cooper, C. Sabbione, F. Hippert, P. Noé, *In situ* observation of the impact of surface oxidation on the crystallization mechanism of GeTe phase-change thin films by scanning transmission electron microscopy, J. Appl. Phys. 122 (2017) 115304. doi:10.1063/1.5002637.

[10] A. Ghalem, A. Hariri, C. Guines, D. Passerieux, L. Huitema, P. Blondy, A. Crunteanu, Arrays of GeTe electrically activated RF switches, 2017 IEEE MTT-S Int. Microw. Work. Ser. Adv. Mater. Process. RF THz Appl. IMWS-AMP 2017. 2018-Janua (2018) 1–3. doi:10.1109/IMWS-AMP.2017.8247380.

[11] N. El-Hinnawy, P. Borodulin, B. Wagner, M.R. King, J.S. Mason, E.B. Jones, S. McLaughlin, V. Veliadis, M. Snook, M.E. Sherwin, R.S. Howell, R.M. Young, M.J. Lee, A four-terminal, inline, chalcogenide phase-change RF switch using an independent resistive heater for thermal actuation, IEEE Electron Device Lett. 34 (2013) 1313–1315. doi:10.1109/LED.2013.2278816.

[12] T. Singh, R.R. Mansour, Chalcogenide Phase Change Material GeTe Based Inline RF SPST Series and Shunt Switches, 2018 IEEE MTT-S Int. Microw. Work. Ser. Adv. Mater. Process. RF THz Appl. IMWS-AMP 2018. (2018) 1–3. doi:10.1109/IMWS-AMP.2018.8457163.

[13] A. Suwardi, S.H. Lim, Y. Zheng, X. Wang, S.W. Chien, X.Y. Tan, Q. Zhu, L.M.N. Wong, J. Cao, W. Wang, Q. Yan, C.K.I. Tan, J. Xu, Effective enhancement of thermoelectric and mechanical properties of germanium telluride: Via rhenium-doping, J. Mater. Chem. C. 8 (2020) 16940–16948. doi:10.1039/d0tc04903d.

[14] J. Li, Z. Chen, X. Zhang, Y. Sun, J. Yang, Y. Pei, Electronic origin of the high

thermoelectric performance of GeTe among the p-type group IV monotellurides, NPG Asia Mater. 9 (2017) e353-8. doi:10.1038/am.2017.8.

[15] S. Perumal, S. Roychowdhury, K. Biswas, High performance thermoelectric materials and devices based on GeTe, J. Mater. Chem. C. 4 (2016) 7520–7536. doi:10.1039/c6tc02501c.

[16] N. Breil, C. Lavoie, A. Ozcan, F. Baumann, N. Klymko, K. Nummy, B. Sun, J. Jordan-Sweet, J. Yu, F. Zhu, S. Narasimha, M. Chudzik, Challenges of nickel silicidation in CMOS technologies, Microelectron. Eng. 137 (2015) 79–87. doi:10.1016/j.mee.2014.12.013.

[17] M.A. Pawlak, J.A. Kittl, O. Chamirian, A. Veloso, A. Lauwers, T. Schram, K. Maex, A. Vantomme, Investigation of Ni fully silicided gates for sub-45 nm CMOS technologies, Microelectron. Eng. 76 (2004) 349–353. doi:10.1016/j.mee.2004.07.037.

[18] J.P. Gambino, E.G. Colgan, Silicides and ohmic contacts, Mater. Chem. Phys. 52 (1998) 99–146. doi:10.1016/S0254-0584(98)80014-X.

[19] E. Assaf, A. Portavoce, K. Hoummada, M. Bertoglio, S. Bertaina, High Curie temperature Mn5Ge3 thin films produced by non-diffusive reaction, Appl. Phys. Lett. 110 (2017). doi:10.1063/1.4976576.

[20] A.N.D. Kolb, N. Bernier, E. Robin, A. Benayad, J.-L. Rouvière, C. Sabbione, F. Hippert, P. Noé, Understanding the Crystallization Behavior of Surface-Oxidized GeTe Thin Films for Phase-Change Memory Application, ACS Appl. Electron. Mater. 1 (2019) 701–710. doi:10.1021/acsaelm.9b00070.

[21] B. Chen, D. De Wal, G.H. Ten Brink, G. Palasantzas, B.J. Kooi, Resolving Crystallization Kinetics of GeTe Phase-Change Nanoparticles by Ultrafast Calorimetry, Cryst. Growth Des. 18 (2018) 1041–1046. doi:10.1021/acs.cgd.7b01498.

[22] M. Libera, M. Chen, Time-resolved reflection and transmission studies of amorphous Ge-Te thin-film crystallization, J. Appl. Phys. 73 (1993) 2272–2282. doi:10.1063/1.353132.

[23] T. Matsushita, T. Nakau, A. Suzuki, M. Okuda, Measurements of activation energy in the initialization process of amorphous GeTe films, J. Non. Cryst. Solids. 112 (1989) 211–214. doi:10.1016/0022-3093(89)90524-3.

[24] X. Sun, E. Thelander, J.W. Gerlach, U. Decker, B. Rauschenbach, Crystallization kinetics of GeTe phase-change thin films grown by pulsed laser deposition, J. Phys. D. Appl. Phys. 48 (2015). doi:10.1088/0022-3727/48/29/295304.

[25] G. Navarro, A. Persico, E. Henaff, F. Aussenac, P. Noe, C. Jahan, L. Perniola, V. Sousa, E. Vianello, B. De Salvo, Electrical performances of SiO2-doped GeTe for phase-change memory applications, IEEE Int. Reliab. Phys. Symp. Proc. (2013) 5–9. doi:10.1109/IRPS.2013.6532100.

[26] A. Fantini, V. Sousa, L. Perniola, E. Gourvest, J.C. Bastien, S. Maitrejean, S. Braga, N. Pashkov, A. Bastard, B. Hyot, A. Roule, A. Persico, H. Feldis, C. Jahan, J.F. Nodin, D. Blachier, A. Toffoli, G. Reimbold, F. Fillot, F. Pierre, R. Annunziata, D. Benshael, P. Mazoyer, C. Vallée, T. Billon, J. Hazart, B. De Salvo, F. Boulanger, N-doped GeTe as performance booster for embedded phase-change memories, Tech. Dig. - Int. Electron Devices Meet. IEDM. (2010) 644–647. doi:10.1109/IEDM.2010.5703441.

[27] M. Gallard, M.S. Amara, M. Putero, N. Burle, M. Richard, C. Mocuta, C. Guichet, O.

Thomas, R.R. Chahine, M. Bernard, P. Kowalczyk, P. Noé, O. Thomas, New insights into thermomechanical behavior of GeTe thin films during crystallization, Acta Mater. 191 (2020) 60–69. doi:10.1016/j.actamat.2020.04.001.

[28] E. Gourvest, B. Pelissier, C. Vallée, A. Roule, S. Lhostis, S. Maitrejean, Impact of Oxidation on Ge2Sb2Te5 and GeTe Phase-Change Properties, J. Electrochem. Soc. 159 (2012) H373–H377. doi:10.1149/2.027204jes.

[29] F. Nemouchi, D. Mangelinck, C. Bergman, P. Gas, U. Smith, Differential scanning calorimetry analysis of the linear parabolic growth of nanometric Ni silicide thin films on a Si substrate, Appl. Phys. Lett. 86 (2005) 041903. doi:10.1063/1.1852727.

[30] P. Gas, F.M. d'Heurle, Formation of silicide thin films by solid state reaction, Appl. Surf. Sci. 73 (1993) 153–161. doi:10.1016/0169-4332(93)90160-D.

[31] H. Mehrer, Diffusion and Point Defects in Elemental Semiconductors, Diffus. Found. 17 (2018) 1–28. doi:10.4028/www.scientific.net/df.17.1.

[32] S. Gaudet, C. Detavernier, A.J. Kellock, P. Desjardins, C. Lavoie, Thin film reaction of transition metals with germanium, J. Vac. Sci. Technol. A Vacuum, Surfaces, Film. 24 (2006) 474–485. doi:10.1116/1.2191861.

[33] J. Perrin Toinin, A. Portavoce, M. Texier, M. Bertoglio, K. Hoummada, First stages of Pd/Ge reaction: Mixing effects and dominant diffusing species, Microelectron. Eng. 167 (2017) 52–57. doi:10.1016/j.mee.2016.11.002.

[34] J. Perrin Toinin, K. Hoummada, M. Bertoglio, A. Portavoce, Origin of the first-phase selection during thin film reactive diffusion: Experimental and theoretical insights into the Pd-Ge system, Scr. Mater. 122 (2016) 22–25. doi:10.1016/j.scriptamat.2016.05.008.

[35] B. De Schutter, K. De Keyser, C. Lavoie, C. Detavernier, Texture in thin film silicides and germanides: A review, Appl. Phys. Rev. 3 (2016). doi:10.1063/1.4960122.

[36] M. Avrami, Kinetics of phase change. I: General theory, J. Chem. Phys. 7 (1939) 1103–1112. doi:10.1063/1.1750380.

[37] M. Avrami, Kinetics of phase change. II Transformation-time relations for random distribution of nuclei, J. Chem. Phys. 8 (1940) 212–224. doi:10.1063/1.1750631.

[38] M. Avrami, Granulation, Phase Change, and Microstructure Kinetics of Phase Change. III, J. Chem. Phys. 9 (1941) 177–184. doi:10.1063/1.1750872.

[39] N. Oueldna, A. Portavoce, M. Bertoglio, A. Campos, A. Kammouni, K. Hoummada, Phase transitions in thermoelectric Mg-Ag-Sb thin films, J. Alloys Compd. 900 (2021) 163534. doi:10.1016/j.jallcom.2021.163534.

[40] S. Raoux, B. Muñoz, H.Y. Cheng, J.L. Jordan-Sweet, Phase transitions in Ge-Te phase change materials studied by time-resolved x-ray diffraction, Appl. Phys. Lett. 95 (2009) 1–4. doi:10.1063/1.3236786.

[41] F. Nemouchi, D. Mangelinck, J.L. Lábár, M. Putero, C. Bergman, P. Gas, A comparative study of nickel silicides and nickel germanides: Phase formation and kinetics, Microelectron. Eng. 83 (2006) 2101–2106. doi:10.1016/j.mee.2006.09.014.

[42] U.R. Evans, The relation between tarnishing and corrosion, Trans. Am. Electrochem. Soc. (1924).

[43] M.J. Starink, The Meaning of the Impingement Parameter .., J. Mater. 36 (2001) 4433–4441.

[44] G. Ruitenberg, A.K. Petford-Long, R.C. Doole, Determination of the isothermal nucleation and growth parameters for the crystallization of thin Ge 2Sb 2Te 5 films, J. Appl. Phys. 92 (2002) 3116–3123. doi:10.1063/1.1503166.

[45] E. Assaf, A. Portavoce, M. Descoins, M. Bertoglio, S. Bertaina, Carbon concentration, Curie temperature, and magnetic resonance field of Mn5Ge3(C) thin films, Materialia. 8 (2019) 100487. doi:10.1016/j.mtla.2019.100487.

[46] A. Portavoce, G. Roland, J. Remondina, M. Descoins, M. Bertoglio, M. Amalraj, P. Eyméoud, D. Dutartre, F. Lorut, M. Putero, Kinetic Monte Carlo simulations of Ge-Sb-Te thin film crystallization, Nanotechnology. 33 (2022) 295601. doi:10.1088/1361-6528/ac6813.

[47] E. Hüger, F. Strauß, J. Stahn, J. Deubener, M. Bruns, H. Schmidt, In-situ Measurement of Self-Atom Diffusion in Solids Using Amorphous Germanium as a Model System, Sci. Rep. 8 (2018) 1–8. doi:10.1038/s41598-018-35915-1.

[48] A. Portavoce, K. Hoummada, F. Dahlem, Influence of interfacial reaction upon atomic diffusion studied by in situ Auger electron spectroscopy, Surf. Sci. 624 (2014) 135–144. doi:10.1016/J.SUSC.2014.02.011.

[49] S. Self-interstitials, Physical review, Nature. 207 (1965) 1238. doi:10.1038/2071238d0.

[50] S. Abhaya, G. Amarendra, G. Venugopal Rao, R. Rajaraman, B.K. Panigrahi, V.S. Sastry, Silicidation in Pd/Si thin film junction-Defect evolution and silicon surface segregation, Mater. Sci. Eng. B Solid-State Mater. Adv. Technol. 142 (2007) 62–68. doi:10.1016/j.mseb.2007.06.024.

[51] J.E. Masse, P. Knauth, P. Gas, A. Charaï, Point defect creation induced by solid state reaction between nickel and silicon, J. Appl. Phys. 77 (1995) 934–936. doi:10.1063/1.359021.

FIGURE captions

Fig. 1: XRD patterns (λ = 0.154 nm) as a function of temperature acquired during in situ isochronal annealing of ~ 0.9 K min^{-1} for a) sample #1 (GeTe layer) and b) sample #2 (Ge/Te bilayer).

Fig. 2: Normalized integrated intensities of diffraction peaks and average grain size (L) during in situ XRD isochronal annealing of ~ 0.9 K min^{-1}: sample #1 (GeTe layer), α-GeTe(202) (open circles); and sample #2 (Ge/Te bilayer), hexagonal-Te(101) (solid squares) and α-GeTe(202) (open squares).

Fig. 3: Normalized integrated intensity $f(t)$ of the α-GeTe(202) diffraction peak versus time recorded during in situ XRD isothermal annealing at various temperatures between 145°C and 190°C: a) and c) sample #1 (GeTe layer); b) and d) sample #2 (Ge/Te bilayer). The solid line in a) and b) corresponds to a fit using the JMAK model with the Avrami exponent n determined from the corresponding signal $\phi = \ln(-\ln(1 - f(t)))$ in c) and d).

Fig. 4: Variations of a) the parameter $\ln(\kappa)$ and b) the nucleation time $\ln(\Delta t)$ according to the inverse of temperature for sample #1 (GeTe layer) and sample #2 (Ge/Te bilayer).

Fig. 5: Cross-section TEM images acquired during in situ sample #2 (Ge/Te) heating from RT to 225°C: a) RT, b) 180°C, c) 205°C, d) 225°C and (e) FFT and reciprocal distances measured in the red dotted rectangle. The blue dotted arrow is used to mark identical location in the different images, and the red solid arrow shows the evolution of a growing GeTe grain within the amorphous Ge layer. The added color highlights the new phase.

Fig. 6: (a), (b) and (c): schematic illustration of nucleation and growth in sample #2 (Ge/Te bilayer, RD); (d) Cross-section TEM images acquired during in situ sample #2 (Ge/Te) heating at 350°C: almost all the layer is crystalline.

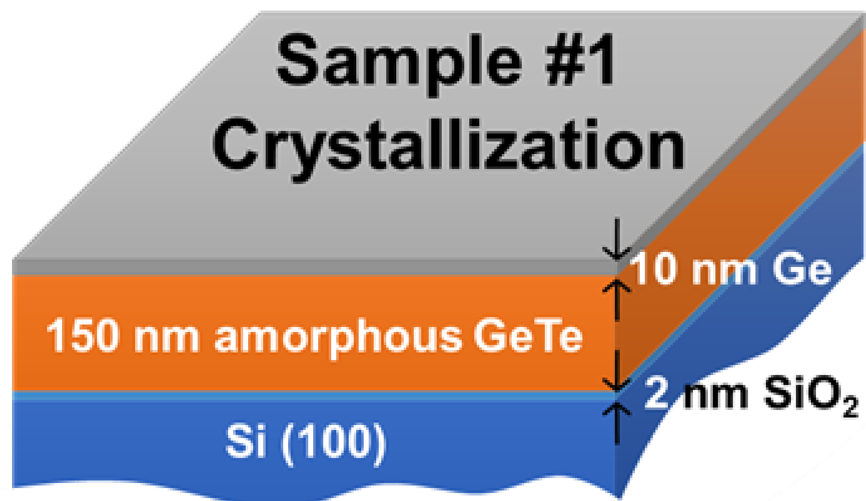

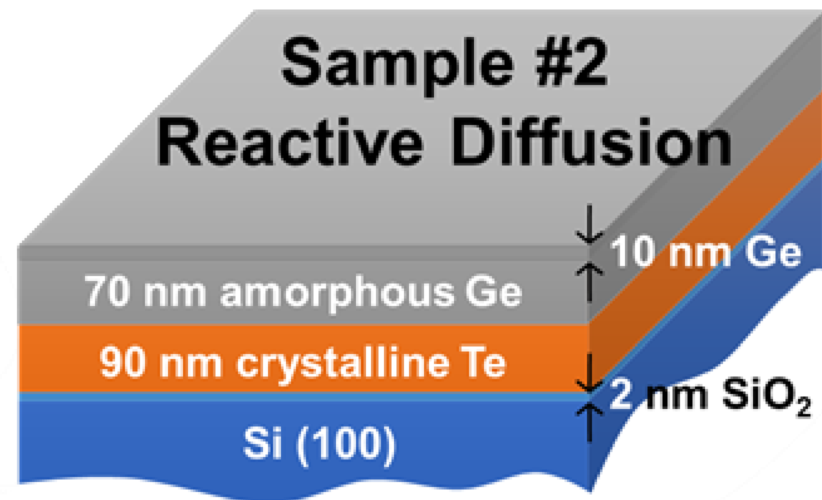

GeTe crystallization

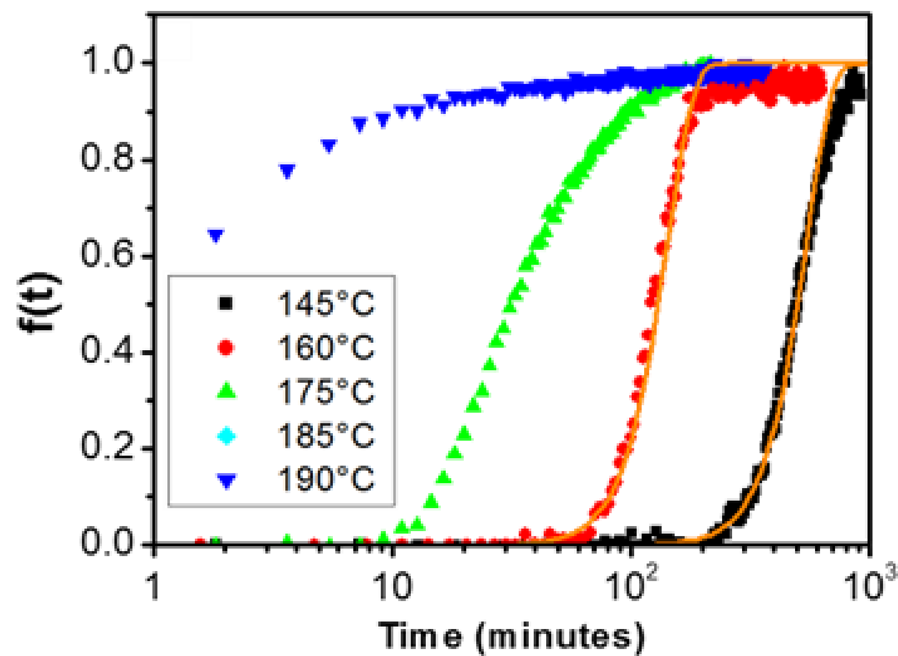

Ge/Te Reactive Diffusion